

## A Linear Analysis of the NCAR CCSM Finite-Volume Dynamical Core

WILLIAM C. SKAMAROCK

*National Center for Atmospheric Research,\* Boulder, Colorado*

(Manuscript received 11 April 2007, in final form 18 September 2007)

### ABSTRACT

The NCAR Community Climate System Model (CCSM) finite-volume atmospheric core uses a C–D-grid discretization to solve the equations of motion. A linear analysis of this discretization shows that it behaves as a D grid to leading order; it possesses the poor response of the D grid for short-wavelength divergent modes, the poor response of the C and D grids for short-wavelength rotational modes, and is only first-order accurate in time and damping. The scheme combines a modified forward–backward time integration for gravity waves with forward-in-time upwind-biased advection schemes, and the solver uses a vector-invariant form of the momentum equations. Other approaches using these equations are considered that circumvent some of the problems inherent in the current approach.

### 1. Introduction

Solvers for the Navier–Stokes equations on the sphere are used as the basis for both climate and global numerical weather prediction models. For these applications there is a growing appreciation of the need for conservative positive-definite and/or monotonic transport of chemical species, aerosols, and moisture. In the National Center for Atmospheric Research (NCAR) Community Climate System Model (CCSM), a second dynamical core incorporating a finite-volume-based solver, described in Lin (2004), was introduced to satisfy the need for conservative scalar transport (Collins et al. 2004, 2006). This hydrostatic primitive equations solver was developed from a shallow-water equations solver (Lin and Rood 1997, hereinafter LR97) that uses a multidimensional transport scheme based on the piecewise parabolic method (PPM; Lin and Rood 1996) that is analyzed in Lauritzen (2007). In this paper we perform a linear analysis of the spatial–temporal discretization used in LR97 to illustrate its characteristics, and we consider alternative approaches.

Linear analyses are often used to determine how well

the structure, propagation, and transport of large-scale rotationally dominated waves (Rossby waves and inertial oscillations), smaller-scale gravity waves (horizontally divergent motions), and inertia–gravity waves are handled in the spatial and temporal discretizations of global atmospheric dynamical cores. Although good linear response characteristics are not sufficient to ensure good performance in more complex nonlinear applications, they are widely regarded as a necessary requirement for the model numerics. In the solvers, discretization choices often represent a trade-off in the accurate representation of one class of motions over another, and this trade-off is quantifiable through the linear analyses. For example, divergent motions (gravity waves) contain little energy at large scales, where rotational modes dominate the kinetic energy spectrum. Models for these applications have usually been constructed with formulations that are most accurate for rotational modes (that may be poorly resolved on coarse grids), and are designed to be stable and perhaps damping for divergent modes. As model resolution is increased, divergent motions begin to become resolved (the mesoscale is where kinetic energy associated with divergent motions is of similar magnitude to that associated with rotational modes). At these resolutions, rotational modes are well resolved while divergent modes are marginally resolved, and hence discretizations are often chosen to accurately represent the marginally resolved divergent modes, with the understanding that rotational modes will be well resolved even with a sub-optimal discretization.

\* The National Center for Atmospheric Research is sponsored by the National Science Foundation.

Corresponding author address: William C. Skamarock, National Center for Atmospheric Research, P.O. Box 3000, Boulder, CO 80307-3000.

E-mail: skamaroc@ucar.edu

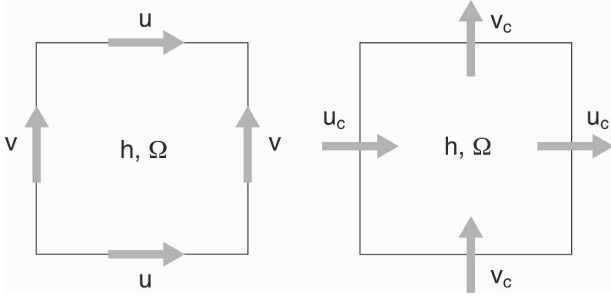


FIG. 1. The two component grids in the C–D-grid model. (left) The D grid and (right) the C grid. Here,  $u$ ,  $v$ , and  $h$  on the D grid are the prognostic variables in the LR97 model, whereas  $\Omega$ , the vorticity, is diagnosed.

The discretization scheme used in the finite-volume (FV) core of the CCSM uses a “reverse engineering” approach (see LR97) in order to accurately resolve both rotational and divergent modes. In the following sections we examine the behavior of this discretization. The temporal–spatial discretization is described in section 2 along with its relationship to standard discretizations. In section 3 we examine the damping properties and stability characteristics for the gravity waves in the solver. We consider the properties of advected gravity waves in section 4 followed by an examination of the nonlinear aspects of the LR97 solver as they relate to other solvers in section 5. A summary is presented in section 6.

## 2. Inertia–gravity wave analysis

We can examine the LR97 solver by considering the linearized shallow-water equations using the standard linearization of the height ( $H + h$ ) and the velocities ( $U + u$  and  $V + v$ ), and we first consider the simplest case with no mean advection,

$$U, V = 0.$$

The appropriately linearized shallow-water equations on an  $f$  plane are

$$h_t + H(u_x + v_y) = 0, \quad (1a)$$

$$u_t - fv + gh_x = 0, \quad \text{and} \quad (1b)$$

$$v_t + fu + gh_y = 0, \quad (1c)$$

where subscripts denote partial differentiation.

The horizontal grid is described in LR97 as a C–D grid and is depicted in Fig. 1; in this paper we follow the spatial grid-staggering naming convention of Arakawa and Lamb (1977). A critical aspect of the C–D-grid scheme is that the velocities on the C-grid component (denoted by subscript  $c$ ) are defined using four-point averages from the D grid *at the beginning of each time step*:

$$u_c = \bar{u}^{xy} \quad \text{and} \quad v_c = \bar{v}^{xy}.$$

The full LR97 time–space discretization for the linearized shallow-water equations is given as follows: First, the midpoint predictor step used in LR97 involves interpolating the velocities from the D grid to the C grid and advancing the C-grid variables over a time step  $\Delta t/2$ :

$$h^* = h^n - (\Delta t/2)HD\bar{n}^{xy}, \quad (2a)$$

$$u_c^* = \bar{u}^{n,xy} - (\Delta t/2)(g\delta_x h^* - fv^n), \quad \text{and} \quad (2b)$$

$$v_c^* = \bar{v}^{n,xy} - (\Delta t/2)(g\delta_y h^* + fu^n), \quad (2c)$$

where  $D$  is the divergence operator

$$\bar{D}^{n,xy} = \delta_x \bar{u}^{n,xy} + \delta_y \bar{v}^{n,xy} = \bar{\delta}_x u^n + \bar{\delta}_y v^n,$$

$\delta_x \phi = (\phi_{x+\Delta x/2} - \phi_{x-\Delta x/2})/\Delta x$  is a difference operator, and the averaging operator  $\bar{\phi}^{xy} = \bar{\phi}^{x,y} = \bar{\phi}^{y,x}$  is an average over  $x$  and  $y$ , where the average is defined as  $\bar{\phi}^x = (\phi_{x+\Delta x/2} + \phi_{x-\Delta x/2})/2$ . The predictor step (2) is followed by the full forward–backward step on the D grid:

$$h^{n+1} = h^n - \Delta t HD_c^*, \quad (3a)$$

$$u^{n+1} = u^n - \Delta t (g\delta_x \bar{h}^{n+1,xy} - fv_c^*), \quad \text{and} \quad (3b)$$

$$v^{n+1} = v^n - \Delta t (g\delta_y \bar{h}^{n+1,xy} + fu_c^*), \quad (3c)$$

where  $D_c^*$  is the divergence using  $(u_c^*, v_c^*)$ . Eliminating the predictor (\*) variables, casting the right-hand-side (rhs) variables at time level  $n$ , and dividing by  $\Delta t$  results in

$$\frac{h^{n+1} - h^n}{\Delta t} = -H(\bar{D}^{n,xy}) + \frac{\Delta t}{2} [-fH(\delta_x v^n - \delta_y u^n) + gH(\delta_x^2 h^n + \delta_y^2 h^n)] + O(\Delta t^2), \quad (4a)$$

$$\frac{u^{n+1} - u^n}{\Delta t} = \bar{f}v^{n,xy} - g\delta_x \bar{h}^{n,xy} - \frac{\Delta t}{2} [f^2 u^n + gf\delta_y h^n - 2gH(\delta_x \bar{D}^{n,xy,xy})] + O(\Delta t^2), \quad \text{and} \quad (4b)$$

$$\frac{v^{n+1} - v^n}{\Delta t} = -\bar{f}u^{n,xy} - g\delta_y \bar{h}^{n,xy} - \frac{\Delta t}{2} [f^2 v^n - gf\delta_x h^n - 2gH(\delta_y \bar{D}^{n,xy,xy})] + O(\Delta t^2). \quad (4c)$$

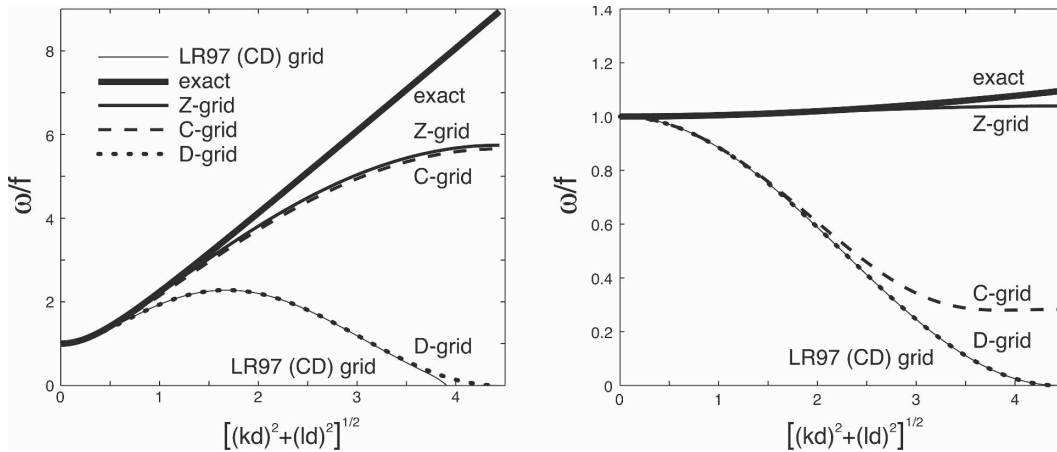


FIG. 2. Dimensionless frequencies of linear inertia-gravity waves for the LR97 C–D grid using the scheme (2)–(3) along with the exact frequency and the Z-, C-, and D-grid frequencies assuming no temporal discretization (from Randall 1994). The results are for waves propagating diagonally across the grid ( $k = l$ ).

The leading-order height-gradient and Coriolis terms in the momentum equations (4b) and (4c) use four-point averaged quantities, and the leading-order velocity divergence term in the height equation (4a) uses four-point averaged velocities. Thus, to first order in time this is a D-grid discretization. As  $\Delta t \rightarrow 0$ , the spatial discretization corresponds exactly to the D grid.

LR97 state that the C–D grid has properties similar to the Z grid analyzed in Randall (1994). Randall’s Z-grid formulation solves the shallow-water equations using vertical vorticity, divergence, and height as prognostic variables, as opposed to horizontal momentum and height. The Z-grid formulation possesses accuracy similar to that of the A grid for inertial oscillations (or any grid for which the velocities are collocated and no averaging is needed for the Coriolis terms in the momentum equations), and it possesses the properties of the C grid for gravity wave motions (the C-grid staggering allows for a very accurate discretization of the divergence and height-gradient terms). The analysis in the previous section shows that LR97’s C–D grid behaves fundamentally as a D grid, and hence it does not appear to possess the properties of Randall’s Z grid. We confirm this behavior by comparing the analytic results found in Randall’s paper with the behavior of LR97’s scheme (2)–(3).

The primary results from Randall (1994) are presented in several plots where the dimensionless inertia-gravity wave frequency  $\omega/f$  is plotted as a function of the dimensionless wavenumbers  $kd$  and  $ld$ , where  $\omega$  is the frequency,  $f$  is the Coriolis parameter,  $k$  and  $l$  are the dimensional wavenumbers, and  $d$  is the grid length. As is standard practice, exact and approximate solutions to the linearized equations are determined by assuming wave solutions of the form  $\phi = \hat{\phi} \exp[i(kx +$

$ly - wt)$ ]. Using (2) and (3) and assuming wave solutions, we can cast the LR97 equations into the form

$$\phi^{n+1} = \mathbf{A}\phi^n, \quad (5)$$

where  $\phi = (h, u, v)^T$  and  $\mathbf{A}$  is the amplification matrix. The eigenvalues of  $\mathbf{A}$  (which we denote as  $\Lambda$ ) are directly related to the frequency and amplitude response in the discrete system:

$$\begin{aligned} \Lambda &= \exp(-i\omega\Delta t), \\ r &= |\Lambda|, \quad \text{and} \\ \omega\Delta t &= \arg(\Lambda). \end{aligned}$$

Three modes are present in the solution: the two inertia-gravity waves and the stationary mode. Figure 2 depicts the results for the two values of  $\lambda/d = (gH)^{1/2}/fd = (2, 0.1)$  examined in Randall (1994) (where  $d \equiv \Delta x$  and  $\lambda$  is the deformation radius in Randall’s notation). For these results we have used  $\Delta t = 300$  s,  $d \equiv \Delta x = 100$  km, and  $f = 10^{-4} \text{ s}^{-1}$ , which, along with  $\lambda$ , are sufficient to specify the two dimensionless parameters that appear in (5),  $f\Delta t$  and  $gH\Delta t^2/d^2$ . Where the gravity wave modes dominate the solution ( $\lambda = 2$ ), the C grid and Randall’s Z grid give the best response. The C–D grid from LR97 gives a frequency response that is essentially that of the D grid except at the highest wavenumbers—where the response is marginally poorer than the poor D-grid response. Where the rotational modes dominate ( $\lambda = 0.1$ ), the C–D-grid and D-grid responses are essentially indistinguishable, and the C, D, and C–D grids all show a very poor response. Thus, LR97’s C–D grid behaves as a D grid, not as Randall’s (1994) Z grid.

The averaging involved in the height-gradient terms in the momentum equations and in the divergence term in the height equation causes the  $2\Delta x$  inertia-gravity

waves to be stationary on the grid as shown in Fig. 2, where the frequency response as a function of dimensionless wavenumber is plotted for waves propagating diagonally across the grid ( $k = l$ ). Essentially, the grid does not see these waves except for some damping of the height field from the time-stepping scheme appearing in the height equation (4a). The CCSM finite-volume core based on LR97's integration scheme (Collins et al. 2004) uses explicit horizontal divergence damping to filter these stationary modes from the momentum fields. Horizontal divergence damping filters gravity waves (Skamarock 2004) and, while perhaps appropriate at large scales where there is little energy in the divergent modes, is inappropriate at smaller scales, beginning at the mesoscale, because of the increasing importance of the divergent motions.

### 3. Damping and stability characteristics for gravity waves

Spatial filtering terms appear in (4a)–(4c) in the form of a second-order spatial filter in the height equation, that is, the term  $(\Delta t/2)gH(\delta_x^2 h^n + \delta_y^2 h^n)$  in (4a), and horizontal divergence-damping terms in the momentum equations, that is, the terms  $\Delta t g H \delta_x \overline{D}^{xy,xy}$  and  $\Delta t g H \delta_y \overline{D}^{xy,xy}$  in (4b) and (4c), respectively. In order to examine the damping and stability characteristics of the scheme for gravity waves, we have analyzed the one-dimensional ( $x$ ) linearized gravity wave equations (1a) and (1b) with  $f = v = 0$ . For the 1D ( $x$ ) case, the C–D grid collapses to an unstaggered (A) grid where  $u$  and  $h$  are defined at the same location. In this case (4a) and (4b) reduce to

$$h^{n+1} = h^n - \Delta t H (\delta_x \overline{u}^{n,x}) + \frac{\Delta t^2}{2} g H (\delta_x^2 h^n) \quad (6a)$$

and

$$u^{n+1} = u^n - \Delta t g (\delta_x \overline{h}^{n,x}) + \Delta t^2 g H (\delta_x^2 \overline{u}^{n,x}). \quad (6b)$$

For comparison, the forward–backward scheme of Mesinger (1977) on an unstaggered (A) grid is

$$h^{n+1} = h^n - \Delta t H (\delta_x \overline{u}^{n,x}) \quad \text{and} \quad (7a)$$

$$u^{n+1} = u^n - \Delta t g (\delta_x \overline{h}^{n+1,x}) \\ = u^n - \Delta t g (\delta_x \overline{h}^{n,x}) + \Delta t^2 g H (\delta_x^2 \overline{u}^{n,x}), \quad (7b)$$

and on the C grid is

$$h^{n+1} = h^n - \Delta t H (\delta_x u^n) \quad \text{and} \quad (8a)$$

$$u^{n+1} = u^n - \Delta t g (\delta_x h^n) + \Delta t^2 g H (\delta_x^2 u^n). \quad (8b)$$

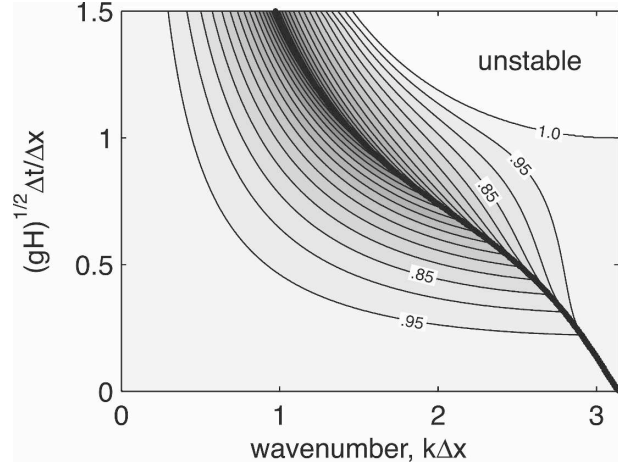


FIG. 3. Amplification factor for 1D linear gravity waves using the LR97 scheme. The contour interval is 0.05 and the shaded region is stable. The thick contour indicates where the eigenvalues change from being complex conjugates, below and to the right, to being real, above and to the left. Modes possessing real eigenvalues do not propagate.

The stability constraint for Mesinger's forward–backward scheme on the A grid is  $\sqrt{gH\Delta t/\Delta x} \leq 2$  and for the C grid is  $\sqrt{gH\Delta t/\Delta x} \leq 1$ . Additionally, the amplification factors are identically equal to 1 in the stable regime—the schemes are neutral. The reduced stability limit for the C grid compared with the A grid is the result of the lack of averaging (and higher accuracy) in the C-grid scheme. Importantly, the diffusion term  $gH\Delta t \delta_x^2 u^n$  in (8b) does not result in damping in the forward–backward scheme—rather it exactly offsets the unstable amplification of the pure forward-in-time scheme. This point can be appreciated by combining (8a) and (8b), which results in

$$\frac{u^{n+1} - 2u^n + u^{n-1}}{\Delta t^2} = gH\delta_x^2 u^n,$$

which is easily recognized as the spatially and temporally centered discretization for the wave equation that is second-order accurate in both time and space and is neutral.

In the LR97 variant of the forward–backward scheme, the third term on the rhs of (6a) is an additional diffusion term that does not appear in the forward–backward schemes (7a) and (8a). This additional term renders the LR97 scheme temporally first-order accurate and it also affects the stability of the scheme. Forming an amplification matrix  $\mathbf{A}$  as in (5) for the scheme (6), we plot the magnitude of the eigenvalues of  $\mathbf{A}$  in Fig. 3. A number of characteristics can be determined from this result. The stability of the LR97 scheme is  $\sqrt{gH\Delta t/\Delta x} \leq 1$  (see the  $2\Delta x$  mode at  $k\Delta x = \pi$ ). Because Mesinger's scheme has a stability limit

$\sqrt{gH\Delta t/\Delta x} \leq 2$ , the inclusion of LR97's predictor step (2) halves the maximum stable time step. Also, the scheme is damping, and shorter-wavelength modes are stationary on the grid as also found for wave propagation in section 2.

#### 4. Waves and advection

The addition of advection will alter the stability of time-integration schemes, and we can examine the impact of advection by including nonzero  $U$  and  $V$  in (1). For simplicity we restrict ourselves to the 1D equations without rotation. The linearized LR97 height equation and the  $u$ -momentum equation in the vector-invariant form are

$$h_t + Uh_x + Hu_x = 0 \quad \text{and}$$

$$u_t + \kappa_x + gh_x = 0,$$

where the linearized kinetic energy gradient  $\kappa_x = \delta_x(Uu)$ . The predictor step in the LR97 scheme can be written as

$$h^* = h^n - \frac{\Delta t}{2} [H\delta_x \overline{u^{n,x}} + U\delta_x Px(U, \Delta t/2; h^n)] \quad (9a)$$

and

$$u_c^* = \overline{u^{n,x}} - \frac{\Delta t}{2} \left\{ g\delta_x h^* + \frac{1}{2} [U\delta_x Px(U, \Delta t/2; \overline{u^{n,x}}) + U\delta_x \overline{\overline{u^{n,x,x}}}] \right\}, \quad (9b)$$

followed by the full time step

$$h^{n+1} = h^n - \Delta t [H\delta_x u_c^* + U\delta_x Px(U, \Delta t; h^n)] \quad (10a)$$

and

$$u^{n+1} = u^n - \Delta t \left\{ g\delta_x \overline{h^{n+1,x}} + \frac{1}{2} [U\delta_x Px(U, \Delta t; u^n) + U\delta_x \overline{\overline{u_c^{*,x}}}] \right\}. \quad (10b)$$

LR97 use the PPM for transport, and we have written the PPM time-integrated flux of tracer  $\phi$  as  $\Delta t[\mathbf{U}Px(\mathbf{U}, \Delta t; \phi)]$ , where  $\phi$  is the fluxed quantity,  $\mathbf{U}$  is the flux velocity, and  $Px^1$  is the operator defining the average value of  $\phi$  integrated over the distance  $U\Delta t$  of the piecewise parabolas (see Carpenter et al. 1990; Woodward and Colella 1984). Note that the linearization of the time-integrated nonlinear flux divergence

$$\Delta t \delta_x [(U + u)Px(U + u, \Delta t; \overline{\phi} + \phi')]$$

is

$$\Delta t \{ U\delta_x [Px(U, \Delta t; \phi')] + \overline{\phi} \delta_x u \},$$

<sup>1</sup> LR97 define the PPM operator  $\chi(\mathbf{U}, \Delta t; \phi) \equiv \mathbf{U}Px(\mathbf{U}, \Delta t; \phi)$ .

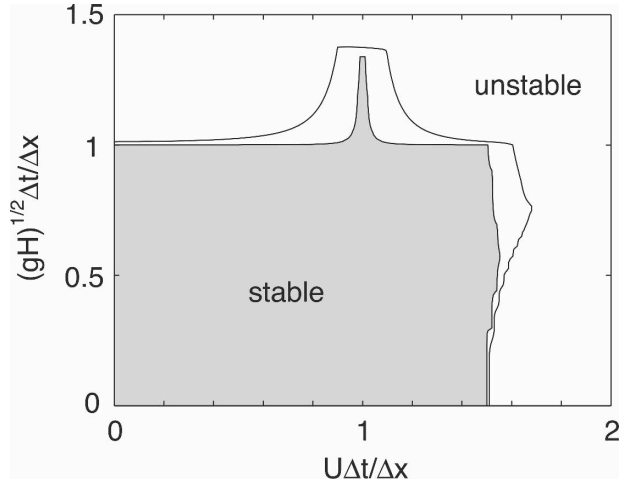


FIG. 4. Stability space for gravity wave propagation with advection for the LR97 scheme. The shaded region is stable, and amplification factor values of 1 and 1.05 are contoured.

hence the form of the rhs of (9a) and (10a). LR97 also use the operator  $Px$  to calculate the kinetic energy in (9b), where the nonlinear term  $\kappa_x$  is discretized as

$$\delta_x \left[ \frac{1}{2} (U + \overline{u^{n,x}}) Px(U + \overline{u^{n,x}}, \Delta t/2; U + \overline{u^{n,x}}) \right],$$

which linearized yields the far rhs terms in (9b) and similarly in (10b).

A linear analysis of the stability of the scheme (9)–(10) is carried out by forming the amplification matrix  $\mathbf{A}$  as in (5). Figure 4 shows the maximum amplitude of the eigenvalues of  $\mathbf{A}$  as a function of the advective and gravity wave Courant numbers. The stability for the discretization (9)–(10) is  $|U\Delta t/\Delta x| \leq 1.5$  and  $|\sqrt{gH\Delta t/\Delta x}| \leq 1$ . The rectangular stable region is a desirable feature of the scheme and can be contrasted with that of a forward–backward scheme coupled with leapfrog advection that would have a stability constraint  $|U\Delta t/\Delta x| + |\sqrt{gH\Delta t/\Delta x}| \leq 1$ , where the Courant numbers are added together in the stability constraint.

LR97 use the predictor step (9) to time center the advective velocities in (10), resulting in a temporally second-order-accurate treatment of advection. Skamarock and Klemp (1992) examined the use of upwind advection schemes (e.g., PPM) with the Mesinger (1977) forward–backward scheme and determined that the upwind schemes were unstable for essentially any nonzero values of both Courant numbers. Thus, steps (9a) and (9b) are crucial to the stability of the LR97 scheme.

#### 5. Nonlinear considerations and alternative approaches

The fully nonlinear shallow-water equations, for the vector invariant form used in LR97, can be written as

$$\begin{aligned} h_t + (uh)_x + (vh)_y &= 0, \\ u_t - \Omega v + \kappa_x + gh_x &= 0, \quad \text{and} \\ v_t + \Omega u + \kappa_y + gh_y &= 0, \end{aligned}$$

where  $u$ ,  $v$ , and  $h$  are here the full variables,  $\Omega = f + v_x - u_y$  is the absolute vorticity, and  $\kappa = (u^2 + v^2)/2$  is the kinetic energy. The LR97 discretization of these equations for the full step (after the predictor step for  $u_c^*$  and  $v_c^*$ ) is given as

$$\begin{aligned} u^{n+1} = u^n - \Delta t \left\{ -v_c^* [Py(v_c^*, \Delta t; \Omega)] + \delta_x \kappa^* \right. \\ \left. + g \delta_x \overline{h^{n+1,xy}} \right\} \quad \text{and} \end{aligned} \tag{11a}$$

$$v^{n+1} = v^n - \Delta t \left\{ u_c^* [Px(u_c^*, \Delta t; \Omega)] + \delta_y \kappa^* + g \delta_y \overline{h^{n+1,xy}} \right\}, \tag{11b}$$

where the terms involving the vorticity are computed using the PPM scheme. The kinetic energy is also defined using the PPM scheme by

$$\kappa^* = \frac{1}{2} \left\{ \overline{u_c^{*y}} [Px(\overline{u_c^{*y}}, \Delta t; u^n)] + \overline{v_c^{*x}} [Py(\overline{v_c^{*x}}, \Delta t; v^n)] \right\}. \tag{12}$$

In (11) and (12) and in what follows, the transport operators  $Px$  and  $Py$  denote the full multidimensional operators used in LR97, described in Lin and Rood (1996) (also see Leonard et al. 1996).

It is illustrative to consider the C-grid version of this discretization,

$$\begin{aligned} u^{n+1} = u^n - \Delta t \left\{ -\overline{v^{*xy}} [Py(\overline{v^{*xy}}, \Delta t; \Omega)] + \delta_x \kappa^* \right. \\ \left. + g \delta_x \overline{h^{n+1}} \right\} \quad \text{and} \end{aligned} \tag{13a}$$

$$\begin{aligned} v^{n+1} = v^n - \Delta t \left\{ \overline{u^{*xy}} [Px(\overline{u^{*xy}}, \Delta t; \Omega)] + \delta_y \kappa^* \right. \\ \left. + g \delta_y \overline{h^{n+1}} \right\}, \end{aligned} \tag{13b}$$

where we have removed the subscript  $c$  because velocities are here defined explicitly at the C-grid points only. The vorticity is naturally defined on the C grid at the corner points, which is at the same location, relative to the velocities  $u$  and  $v$ , as on the D grid. Recalling that to first order  $u_c^* = \overline{u^{xy}}$  and  $v_c^* = \overline{v^{xy}}$  in the LR97 scheme, we see immediately that (11) and (13) are nearly identical in their treatment of the vorticity term, and the obvious difference is their treatment of the height-gradient terms in (11a) and (13a). The kinetic energy terms, however, are also treated differently. The kinetic energy on the C grid is defined as

$$\kappa^* = \frac{1}{2} \left[ \overline{u^{*x}} Px(\overline{u^{*x}}, \Delta t; u^n) + \overline{v^{*y}} Py(\overline{v^{*y}}, \Delta t; v^n) \right]. \tag{14}$$

The C-grid kinetic energy calculation involves less averaging when compared with LR97; a four-point average is used to compute  $u_c^*$  in (12) while no averaging is needed for  $u^*$  in (14).

If we disregard the height-gradient terms, it is possible to discretize the momentum equations on the C grid exactly as in LR97 (recall that the C and D grids are identical except for the location of the height points). On the C grid this would require predicting  $u_d^*$  and  $v_d^*$  as opposed to having all predicted velocities at their C-grid locations as given in (13) and (14). This approach would increase the leading-order truncation error terms associated with the kinetic energy gradients, and would require averaging the height-gradient terms in the  $u_d^*$  and  $v_d^*$  equations, but not in the  $u^{n+1}$  and  $v^{n+1}$  equations. Overall, more averaging is introduced and truncation error is increased, but not as much as that associated with the full LR97 scheme.

The increased averaging in the LR97 scheme compared with a pure C-grid scheme does have the beneficial aspect of increasing the stability region for gravity wave propagation from  $|\sqrt{gH\Delta t/\Delta x}| \leq 1/2$  (the C-grid constraint for an LR97 type integration) to  $|\sqrt{gH\Delta t/\Delta x}| \leq 1$ . The detrimental effects of using the LR97 D grid are that the grid does not see  $2\Delta x$  modes in the momentum fields and height fields, as discussed in section 2. The nonlinear terms in (11) and (12) associated with the use of PPM transport may provide some damping of the  $2\Delta x$  modes, although the need for horizontal divergence damping suggests that PPM damping, even with monotonic limiters, is not sufficient. It should also be noted that the PPM scheme is only first-order accurate (it reverts to the first-order upwind scheme) when the limiters are active.

When developing solvers that work well for both large and small scales, we wish to resolve both the rotational and divergent modes as accurately as possible throughout the discrete wavenumber range, and it is the highest wavenumbers (shortest wavelengths) that are the most problematic. In comparison with the LR97 discretization, other approaches using the vector-invariant form possess better phase and amplitude responses for the short wavelength inertia-gravity waves than the LR97 scheme. For example, Randall's (1994) Z grid possesses both the desirable properties of the C grid for divergent modes and of an unstaggered grid for inertial oscillations, as indicated in Fig. 2. It uses vorticity and divergence for prognostic variables as opposed to momentum and thus requires the solution of

an elliptic equation each time step, so the simplicity of a fully explicit time step, used in LR97, is lost. The ZM grid, examined by Ringler and Randall (2002), uses momentum and height equations and has properties similar to the Z grid. Both components of velocities are defined at twice as many points than the height field; hence a computational mode exists that needs filtering.

Most mesoscale models, and many global models, use a C-grid discretization because of its accurate discretization for divergent modes. Adcroft et al. (2004) describe a hydrostatic solver for both ocean and atmosphere general circulation models using the vector-invariant form of the momentum equations and a C-grid discretization. As discussed in section 2, the C grid suffers from poor resolution of inertial oscillations. Adcroft et al. (1999) design a scheme that solves the momentum equations using both a C and a D grid that resolves this problem. Importantly, the D-grid velocities are carried over between time steps; hence this approach does not suffer from the deficiencies of the LR97 scheme. The introduction of a second set of velocities, however, introduces a computational mode that must be filtered. The solver makes use of an incompressibility constraint; thus, an elliptic equation is solved each time step and the solution procedure cannot be directly compared to LR97's explicit scheme.

Tripoli (1992) describes a model that solves the fully compressible nonhydrostatic equations using momentum equations cast in a vector-invariant form. The model uses a C grid and a time-split scheme that integrates terms associated with the high-frequency gravity and acoustic waves with a small time step and all other (lower frequency) terms with a larger time step. This is a mesoscale/cloud-scale model and it is typically configured such that the large-scale inertial modes are well resolved and no problems with inertial oscillations are reported.

General approaches to improving the C-grid response for inertia-gravity waves are given by Nechaev and Yaremchuk (2004) and Dobricic (2006) in the context of ocean modeling, where typical horizontal grid lengths are often not much smaller than the Rossby radius. The Nechaev and Yaremchuk (2004) scheme makes use of an averaged symmetrized shifts approximation (ASSA), which results in damping of the grid-scale noise associated with the four-point averaging of the velocities for the C-grid computation of the Coriolis term, in addition to increased accuracy for the longer waves. The Dobricic (2006) scheme uses a different averaging of the velocity components in the Coriolis terms to improve the accuracy of the inertial frequencies, although the scheme does not improve the response for the shortest waves.

As noted by Nechaev and Yaremchuk (2004), there is a nonzero null space for the averaging operator used on the velocities for the C-grid Coriolis terms; thus, the C-grid solutions are prone to noise when the horizontal grid spacing is not significantly smaller than the Rossby radius. Improvements to the C-grid response need to remove or damp the nonzero null space in addition to increasing the accuracy of modes that can realistically be resolved by a finite-difference or finite-volume scheme. The LR97 scheme does not address the D-grid problems with the inertial modes (which it shares with the C grid), nor the D-grid problem with the divergent modes (for which the CCSM core makes use of horizontal divergence damping). The Adcroft et al. (1999) scheme removes the C-grid nonzero null space only to insert another and proposes filters for the new computational mode. The Nechaev and Yaremchuk (2004) scheme directly filters the null space. Dobricic (2006) does not directly filter the null space, but he states in his conclusions that the scale-selective filters used in the full models should be sufficient to address the noise, especially if the improved schemes further concentrate the errors in the shortest wavelengths. Thus higher accuracy, combined with physically appropriate, scale-selective filtering, appears to be the necessary component to improved model discretizations with regard to the representation of inertia-gravity waves.

## 6. Summary

Various linear analyses, and inspection of the nonlinear formulation, of the LR97 scheme for integrating the shallow-water equations lead us to the following conclusions:

- 1) To first order in time, the LR97 discretization behaves as a D grid. The leading-order height-gradient and Coriolis terms in the momentum equations (4b) and (4c) use four-point averaged quantities, and the leading-order velocity divergence term in the height equation (4a) uses four-point averaged velocities. As  $\Delta t \rightarrow 0$ , the spatial discretization is exactly that of the D grid.
- 2) The scheme does not possess the desirable properties of Randall's Z grid as outlined in Randall (1994). It possesses the poor C-grid response for marginally resolved rotational modes, and the poor D-grid response for marginally resolved divergent modes.
- 3) The scheme is temporally first-order accurate and damping for horizontally divergent motions (gravity waves).
- 4) The modified LR97 forward-backward integration

scheme has a stability region twice as restrictive as Mesinger's forward-backward scheme for its spatial discretization, and is less accurate.

- 5) The LR97 scheme possesses a desirable stability condition, for the wave propagation coupled with advection, of  $|U\Delta t/\Delta x|$ ,  $|\sqrt{gH\Delta t/\Delta x}| \leq \text{constant}$ , as opposed to the more restrictive constraint  $|U\Delta t/\Delta x| + |\sqrt{gH\Delta t/\Delta x}| \leq \text{constant}$ .
- 6) The first step in the LR97 scheme that predicts the midpoint velocity is necessary for scheme stability. The forward-backward scheme of Mesinger (1977) cannot be used directly with the Lin and Rood (1996) transport.
- 7) The C-grid formulation, using the vector-invariant momentum equations in LR97 has a similar treatment of vorticity, and a more accurate representation of the kinetic energy gradient, compared with the LR97 C-D-grid formulation.

The deficiencies of the LR97 scheme are partially alleviated by using a C grid, particularly deficiencies associated with divergent modes, and for grid spacings much smaller than the Rossby radius, deficiencies in the C-grid representation of the Coriolis terms vanish because little rotational energy is contained near the grid scale. In atmospheric simulation, divergent modes become increasingly important as grid resolutions reach into the mesoscale, and horizontal divergence damping (as needed in the LR97-based models) is no longer appropriate for filtering at these resolutions. For these reasons, we recommend that the C grid be used in place of the LR97 C-D grid. The C grid is used in most mesoscale and cloud-scale atmospheric models, and in many global atmospheric models as well as many ocean models. In applications where the grid spacing is not much smaller than the Rossby radius, a number of approaches exist to improve the inertial response of the C grid. These approaches (e.g., Adcroft et al. 1999; Nechaev and Yaremchuk 2004; Dobricic 2006) rely on increasing the accuracy of the inertial mode response and filtering the nonzero null space that results from averaging the velocity components in the Coriolis terms. Last, all atmospheric models need filters because of the down-scale nonlinear cascade of energy and enstrophy. These filters are typically designed to be very scale selective so as to maximize the resolving power of the models, and they do not preferentially target important dynamical modes (e.g., horizontally divergent modes in high-resolution applications).

*Acknowledgments.* I thank Joseph Klemp, Peter Lauritzen, and two anonymous reviewers for their careful reviews of this manuscript.

## REFERENCES

- Adcroft, A., C. Hill, and J. Marshall, 1999: A new treatment of the Coriolis terms in C-Grid models at both high and low resolutions. *Mon. Wea. Rev.*, **127**, 1928–1936.
- , J.-M. Campin, C. Hill, and J. Marshall, 2004: Implementation of an atmosphere-ocean general circulation model on the expanded spherical cube. *Mon. Wea. Rev.*, **132**, 2845–2863.
- Arakawa, A., and V. R. Lamb, 1977: Computational design of the basic dynamical processes of the UCLA general circulation model. *Methods Comput. Phys.*, **17**, 173–265.
- Carpenter, R. L., K. K. Droegemeier, P. R. Woodward, and C. E. Hane, 1990: Application of the piecewise parabolus method (PPM) to meteorological modeling. *Mon. Wea. Rev.*, **118**, 586–612.
- Collins, W. D., P. J. Rasch, B. A. Boville, J. J. Hack, J. R. McCaa, D. L. Williamson, J. T. Kiehl, and B. Briegleb, 2004: Description of the NCAR Community Atmosphere Model (CAM 3.0). NCAR Tech. Note NCAR/TN464+STR, 226 pp.
- , and Coauthors, 2006: The formulation and atmospheric simulation of the Community Atmosphere Model Version 3 (CAM3). *J. Climate*, **19**, 2144–2161.
- Dobricic, S., 2006: An improved calculation of Coriolis terms on the C grid. *Mon. Wea. Rev.*, **134**, 3764–3773.
- Lauritzen, P., 2007: A stability analysis of finite-volume advection schemes permitting long time steps. *Mon. Wea. Rev.*, **135**, 2658–2673.
- Leonard, B. P., A. P. Lock, and M. K. Macvean, 1996: Conservative explicit unrestricted-time-step multidimensional constancy-preserving advection schemes. *Mon. Wea. Rev.*, **124**, 2588–2606.
- Lin, S.-J., 2004: A vertically Lagrangian finite-volume dynamical core for global models. *Mon. Wea. Rev.*, **132**, 2293–2307.
- , and R. B. Rood, 1996: Multidimensional flux form semi-Lagrangian transport schemes. *Mon. Wea. Rev.*, **124**, 2046–2070.
- , and —, 1997: An explicit flux-form semi-Lagrangian shallow-water model on the sphere. *Quart. J. Roy. Meteor. Soc.*, **123**, 2477–2498.
- Mesinger, F. M., 1977: Forward-backward scheme and its use in a limited area model. *Contrib. Atmos. Phys.*, **50**, 200–210.
- Nechaev, D., and M. Yaremchuk, 2004: On the approximation of the Coriolis terms in C-grid models. *Mon. Wea. Rev.*, **132**, 2283–2289.
- Randall, D. A., 1994: Geostrophic adjustment and the finite-difference shallow-water equations. *Mon. Wea. Rev.*, **122**, 1371–1377.
- Ringler, T. D., and D. A. Randall, 2002: The ZM grid: An alternative to the Z grid. *Mon. Wea. Rev.*, **130**, 1411–1422.
- Skamarock, W. C., 2004: Evaluating mesoscale NWP models using kinetic energy spectra. *Mon. Wea. Rev.*, **132**, 3019–3032.
- , and J. B. Klemp, 1992: The stability of time-split numerical methods for the hydrostatic and the nonhydrostatic elastic equations. *Mon. Wea. Rev.*, **120**, 2109–2127.
- Tripoli, G. J., 1992: A nonhydrostatic mesoscale model designed to simulate scale interaction. *Mon. Wea. Rev.*, **120**, 1342–1359.
- Woodward, P. R., and P. Colella, 1984: The numerical simulation of two-dimensional fluid flow with strong shocks. *J. Comput. Phys.*, **54**, 115–173.